JGR Space Physics

RESEARCH ARTICLE
10.1029/2024JA033415

Estimating Solar Wind Charge Exchange Generated Soft X-Rays in the Jovian Magnetosheath

Fenn Leppard[1], Atlas Patrick[2], Licia Ray[3], William R. Dunn[4], H. Todd Smith[5], Zhonghua Yao[1], Binzheng Zhang[1], TianRan Sun[6], and Chi Wang[6]

[1]Department of Earth and Planetary Sciences, The University of Hong Kong, Pokfulam, Hong Kong, [2]Department of Mathematics, Physics and Electrical Engineering, Northumbria University, Newcastle upon Tyne, UK, [3]Department of Physics, Lancaster University, Lancaster, UK, [4]Department of Physics, University College London, London, UK, [5]Johns Hopkins Applied Physics Laboratory, Laurel, MD, USA, [6]National Space Science Center, Chinese Academy of Sciences, Beijing, China

Key Points:

- Solar Wind Charge eXchange (SWCX) soft x-ray emissions from the Jovian magnetosheath are 4–5 orders of magnitude weaker than the diffuse soft x-ray background
- An X-ray imager at Jupiter would be able to perform observations of other x-ray bright sources inside or outside of the magnetopause
- We use a combination of numerical and magnetohydrodynamic simulation derived results, along with in-situ data to estimate SWCX emissions at Jupiter

Correspondence to:
F. Leppard,
fleppard@connect.hku.hk

Citation:
Leppard, F., Patrick, A., Ray, L., Dunn, W. R., Smith, H. T., Yao, Z., et al. (2025). Estimating solar wind charge exchange generated soft x-rays in the Jovian magnetosheath. *Journal of Geophysical Research: Space Physics*, *130*, e2024JA033415. https://doi.org/10.1029/2024JA033415

Received 16 OCT 2024
Accepted 10 JUN 2025

Author Contributions:
Conceptualization: Licia Ray, William R. Dunn
Formal analysis: Fenn Leppard, Atlas Patrick, H. Todd Smith
Investigation: Fenn Leppard, Atlas Patrick
Methodology: Fenn Leppard, Atlas Patrick, H. Todd Smith
Resources: H. Todd Smith
Supervision: Licia Ray, William R. Dunn, Zhonghua Yao, Binzheng Zhang
Visualization: Fenn Leppard, Atlas Patrick
Writing – original draft: Fenn Leppard, Atlas Patrick
Writing – review & editing: Fenn Leppard, Atlas Patrick, Licia Ray, William R. Dunn, H. Todd Smith, Zhonghua Yao, Binzheng Zhang, TianRan Sun, Chi Wang

Abstract Solar Wind Charge eXchange (SWCX) generated soft x-rays are used extensively to study the interfaces between charged and neutral particles throughout the solar system. This paper outlines the development of a model of Jupiter's magnetosheath using magnetohydrodynamic derived boundary equations and a combination of in situ Juno measurements and numerical models for neutral and charged particle distributions. These are then used to model SWCX emissions in the Jovian magnetosheath for the OVII triplet to determine if the magnetosheath could be imaged in a similar fashion to the planned SMILE mission at Earth. We determine that whole detector counts per minute range from $10^{-5\pm1}$ to $10^{-3\pm1}$ for various spacecraft, which are 4–5 orders of magnitude weaker than the diffuse soft x-ray background and, as such, argue that it is infeasible to study the x-ray emissions from the Jovian magnetosheath. Magnetosheath SWCX emissions would contribute a negligible amount to the diffuse background when performing higher signal x-ray observations at Jupiter such as x-ray aurora, emissions from the Io plasma torus, and fluorescence emissions from the Jovian moons in an in-situ setting, indicating that an x-ray instrument would be capable of performing observations of these brighter x-ray targets either inside or outside of the magnetopause.

1. Introduction

Before the discovery of soft x-ray emissions from comet Hyakutake by ROSAT in 1996 (Lisse et al., 1996), the only known planets that emitted x-rays were Jupiter and Earth (Barbosa, 1990; Bhardwaj & Gladstone, 2000; Bhardwaj et al., 2007; Robertson et al., 2006). Subsequently, the search for more x-ray sources in the heliosphere expanded, and x-ray emissions have been observed from the rings, plasma tori, surfaces and atmospheres of solar system planets and moons as well as many other comets and a puzzling detection from the Kuiper Belt (Bhardwaj et al., 2005; Branduardi-Raymont et al., 2010; Dennerl, 2002; Dennerl et al., 2002; Dunn, 2022; Elsner et al., 2002; Lisse et al., 2017; Nulsen et al., 2020). These emissions were proposed to originate from charge exchange between neutrals and heavy solar wind ions by Cravens (1997). In this process, the collision between the two particles triggers the exchange of an electron from the neutral to the high charge-state ion, leaving the ion in an excited state. The consequent de-excitation results in the emission of an extreme ultraviolet (EUV) or x-ray photon.

The joint ESA and CAS mission SMILE (Solar wind Magnetosphere Ionosphere Link Explorer) is set to launch in 2025 and will explore SWCX emissions from Earth's magnetosheath (Branduardi-Raymont et al., 2018; Raab et al., 2016; Sembay et al., 2024; Wang & Branduardi-Raymond, 2018; Wang & Sun, 2022). SWCX emissions can be used to study the position and variation of the magnetosheath and reveal key characteristics of the region, such as temperature, velocity, density, and composition (Brown et al., 2009; Carter & Sembay, 2008; Carter et al., 2011; Cravens et al., 2001; Guo et al., 2024; Küntz et al., 2024; Ness et al., 2001; Porquet et al., 2010; Sun et al., 2019, 2020; Zhang et al., 2022). These global measurements, derived from images and their spectral characteristics, are vital to help us improve our understanding of planetary magnetosheaths and can be used to verify the accuracy of theoretical models and simulations of the magnetosheath by capturing dynamic variability over a broad region of the magnetosphere.

The nature of the interaction between the Jovian magnetosphere and the solar wind is widely debated (e.g., Bagenal & Delamere, 2011; Cowley et al., 2008; Delamere & Bagenal, 2010; McComas & Bagenal, 2007). But the solar wind is known to play a significant role in driving variation in Jupiter's aurorae and radio emissions (e.g.,

Dunn et al., 2016; Dunn, Gray, et al., 2020; Gurnett et al., 2002; S. Hess et al., 2012; S. L. Hess et al., 2014; Nichols et al., 2009, 2017; Weigt et al., 2020; Wibisono et al., 2020; Yao et al., 2022). With sufficient temporal and spatial resolution, direct global observations of the Jovian magnetosheath would help to address long-standing questions as to the nature of the solar wind interaction at Jupiter such as the extent and location of reconnection sites (Desroche et al., 2012) and magnetospheric breathing as a function of internal plasma pressure and external solar wind drivers (Feng et al., 2023).

Jupiter has an extensive history of x-ray observations; the first being the observation of x-rays produced by Iogenic sulfur and oxygen precipitating into the Jovian atmosphere in 1983 (Metzger et al., 1983). This was followed by ROSAT observing both polar and equatorial emissions from the planet in 1994 (Waite Jr et al., 1994); detections of emissions from the Galilean moons and Io plasma torus and detailed studies of the Jovian atmospheric and auroral emissions by XMM-Newton, Chandra and NuSTAR and detection of Jupiter's radiation belt x-ray emissions by Suzaku (e.g., Branduardi-Raymont et al., 2004, 2007a, 2007b, 2008; Dunn, 2022; Dunn et al., 2016, 2017; Dunn, Branduardi-Raymont et al., 2020; Dunn, Gray, et al., 2020; Elsner et al., 2002, 2005; Ezoe et al., 2010; Gladstone et al., 2002; Mori et al., 2022; Nulsen et al., 2020; Wibisono et al., 2020, 2021, 2023). One of the distinct features of Jupiter's x-ray emission is the strong pulsation of x-ray aurorae, first discovered by Gladstone et al. (2002). The periodicities vary from 10 to 40 min, and sometimes show different periodicities in both hemispheres (Dunn et al., 2017). The periodicity was suggested to be driven by electromagnetic ion cyclotron waves, likely driven by large scale magnetospheric compressional waves (Yao et al., 2021), but the driver for these magnetospheric waves is not yet clear. Global x-ray observations of the Jovian magnetosheath could reveal a possible driver. Despite this extensive history and the diverse interests in Earth's magnetosheath x-rays, the Jovian magnetosheath is yet to be actively observed by an x-ray instrument.

Therefore, this study aims to determine if observing the Jovian magnetosheath using SWCX emissions is viable by using our current understanding of neutral populations and in situ data from Juno and models of the structure of the magnetosheath. This is a much simpler approach compared to terrestrial studies (e.g., Guo et al., 2024; Robertson et al., 2006; Samsonov et al., 2023) as we are trying to determine its viability based on approximations due to limited in-situ data from the Jovian magnetosheath. If SWCX observations are possible the case can be made for a future Jupiter mission with a EUV/x-ray instrument to observe the region and map the magnetosheath to determine its composition, density, and temperature on a global scale.

2. Model Details

SWCX emissions are calculated for each point that lies in the magnetosheath using

$$I_j = \int P_{sqj} dl = \sum_n \int n_n n_q v_{rel} \sigma_{sqn} b_{sqj} d\Omega dl / 4\pi \quad (1)$$

where I_j is the emission intensity of SWCX photons for transition j for species s in charge state q along a line-of-sight dl. P_{sqj} is the volume emission rate, n_n and n_q are the number densities for the neutral and ion species, respectively, v_{rel} is the relative velocity between the targets, σ_{sqn} is the interaction cross section and b_{sqj} is the branching ratio (Sibeck et al., 2018).

Consequently, our model has the following constituents: (a). A magnetopause model to guide the shape of the emission region; (b). Solar wind abundances in the magnetosheath from in situ spacecraft measurements; (c). Models of the neutral populations in the magnetosheath; and (d). Branching ratios and atomic cross sections for the generation of x-rays from the neutral-ion interactions in the Jovian magnetosheath.

2.1. Magnetopause Model

The coordinate basis of the model is equivalent to the geocentric solar magnetospheric system. X points sun-ward, Z along the Jovian spin axis in the direction of positive angular momentum, and Y completes a right-handed set pointing toward dusk with Jupiter centered on the origin, henceforth referred to as JSM. The boundary surfaces of the bow shock and magnetopause are defined using a collection of curves derived by Joy et al. (2002) through a least square fitting process against boundaries produced by the Ogino-Walker magnetohydrodynamic (MHD) simulation at Jupiter (Ogino et al., 1998). This MHD simulation assumes that the solar wind flow is orthogonal to

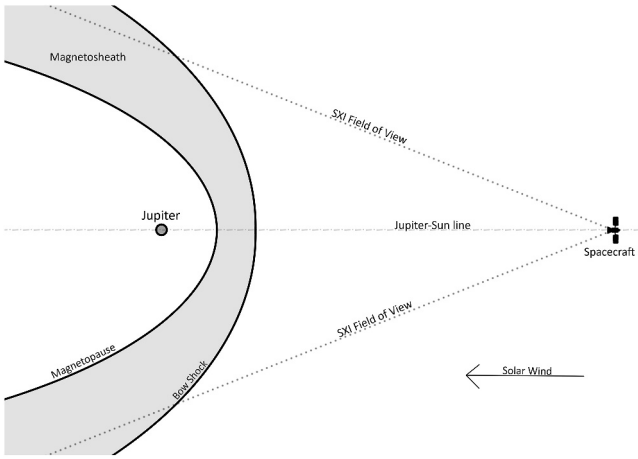

Figure 1. Geometry of the magnetosheath. A soft x-ray imager is placed upstream 744 R_J to capture the main sheath emission region.

the magnetic field and the magnetic field is a spin axis aligned dipole. The bow shock and magnetopause boundaries for different solar wind dynamic pressures are thusly described using

$$z^2 = A + Bx + Cx^2 + Dy + Ey^2 + Fxy \quad (2)$$

where the coefficients are provided in Figure 3 of Joy et al. (2002). We first model the magnetosheath in two dimensions in the $z = 0$ plane and then extend to three dimensions. Figure 1 shows the geometry of the system in the equatorial plane.

2.2. Solar Wind Abundance Measurements

Juno has measured the dawn magnetosheath proton density in situ (Ranquist et al., 2019). A constant proton density of 0.98 cm^{-3}, the average value from the Juno dawn magnetosheath survey, is imposed for 3D calculations and used as a maximum density for the 2D description. This value is very close to the median density in the Jovian magnetosheath which is not the case in the terrestrial magnetosheath. To calculate the density of high charge state oxygen ions, we use the ratio of oxygen to hydrogen ions to calculate a total oxygen ion content in the solar wind (Bochsler, 2007; Lodders, 2019). Using the fraction of O^{7+} ions in the solar wind obtained using charge state ratios measured by ACE (Stone et al., 1998) allows us to calculate the O^{7+} content. To first order, we assume that all the oxygen ions in the solar wind are either O^{6+}, O^{7+}, or O^{8+} and average over fast and slow wind conditions. Although the slow solar wind typically has a higher ratio of O^{7+} ions to O^{6+} ions (Sibeck et al., 2018), this approximation is sufficient for our study and its implications will be discussed in Section 3.

A benefit of using a 2D model is the ability to easily impose structure in the magnetosheath ion density, temperature and bulk velocity. Gradients are applied using best-fits to the contours from Stahara et al. (1989) and Siscoe and Summers (1981). The equations describing the contour fits are as follows: (a). Proton density $\left(m^{-3}\right)$: $\rho = 5r + \left(0.98 \times 10^6\right)$; (b). Ion temperature (eV): $T = -0.07r + 197$; (c). Bulk velocity (ms^{-1}): $v_B = -250r + 348000$. The constants in each equations are the average measured values from Ranquist et al. (2019), and the equations were determined using contour plots from Stahara et al. (1989). There is naturally a degree of uncertainty between the fits and original analyses. However, exploring the effect of a non-uniform magnetosheath on SWCX offers substantial insight into the viability of a SMILE-like mission at Jupiter. Future work could investigate applying updated magnetosheath data to determine more accurate structure.

2.3. Neutral Populations in the Magnetosheath

The main sources of neutrals within the Jovian system are Io and Europa which form an exponential disk in the equatorial plane of the magnetosphere. Radial profiles of the neutral density inside of 50 R_J were determined using a validated 3D Monte Carlo self-consistent neutral particle computational model that has been applied extensively to the Saturn (Smith & Richardson, 2021; Smith et al., 2004, 2007, 2010, 2018) and Jupiter system (Smith et al., 2019, 2022). This model accounts for the gravitational effects of Jupiter and all major satellites, as well as particle interaction processes including electron impact ionization and dissociation, photoionization and photo-dissociation, recombination, charge exchange, neutral-neutral collisions, collision with Jupiter and its satellites, as well as escape from the Jovian system. The model ejects weighted particles from each magnetospheric source and tracks their trajectories under the influence of the above processes. In the case of molecular source particles, the model also generates and tracks resulting dissociated species particles. The particles are accumulated to derive the 3D spatial distribution of all neutral particles (SO_2, SO, S, H_2O, OH, O, O_2, H, and H_2) and their resulting ions. We extracted 3D neutral density results from the Smith et al. (2022) study which represents average magnetospheric conditions during an Io "quiet time" period, shown as the data points in Figure 2. This study also applied the average plasma density and temperature conditions as shown in Appendix B of Smith et al. (2022). Note that although hydrogen is the relevant species for this work, we must also include all major neutral species and sources because neutral particles can impact each other through complicated interaction pathways.

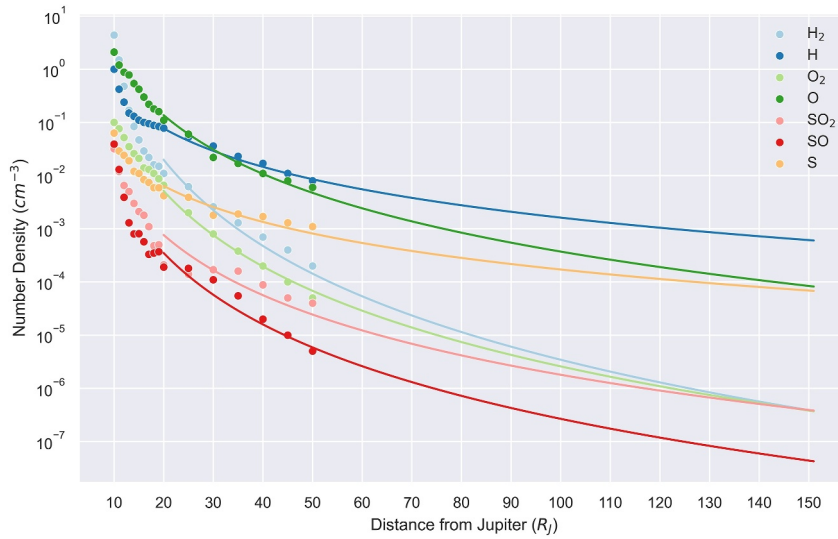

Figure 2. Radial distribution of neutrals in the Jovian system. Dots are data points from a neutral particle computational model applied to the Jovian system. The lines show the best fit to data outside of 20 R_J.

These profiles were extrapolated to 250 R_J by fitting a power law function to each neutral species, with the neutral density in the equatorial plane out to 150 R_J shown in Figure 2. Atomic Hydrogen is the main species considered in the magnetosheath as it dominates the distribution outside of 55 R_J. We approximate the density of Hydrogen in the equatorial plane as

$$n_{H_{eq}}(r) = 102.1 r^{-2.4} \ (r > 14 R_J) \tag{3}$$

where r is the radial distance from Jupiter by fitting a function to the model data, as seen in the dark blue line/points in Figure 2.

Charge exchange is the dominant process that provides neutral particles with enough energy to form the extended neutral cloud. The distribution of neutrals off the equatorial plane is constrained through consideration of the plasma disc scale height as most neutrals in the magnetosheath will be generated by charge exchange with the plasma disc. The imposed distribution is

$$n_H(r,z) = n_{H_{eq}}(r) \exp -(z/2.0)^2 \tag{4}$$

where z is the distance from the equatorial plane. This follows the formulation for the 2.0 R_J inner magnetospheric plasma scale height presented by (Bagenal & Delamere, 2011). Given the variation of the outer magnetospheric plasma conditions and lack of published plasma scale heights for this region, we apply the 2.0 R_J scale height of the neutral distributions to further distances from Jupiter.

2.4. Branching Ratios and Atomic Cross Sections for X-Ray Production in the Magnetosheath

We focus our calculation on soft x-ray emission from the Oxygen triplet, which is predominantly generated by charge exchange between neutral hydrogen atoms and O^{7+} ions originating in the solar wind. This interaction was chosen as oxygen is the most abundant heavy ion species in the solar wind (Lodders, 2019), and neutral hydrogen is likely to be the dominant neutral species in the magnetosheath. The dominant soft x-ray emission lines from the CHANDRA comet survey are the OVII triplet (Bodewits, D. et al., 2007) comprised of the forbidden line (z: $1s^2\ ^1S_0$ $1s2s\ ^3S_1$, 561.1 eV), the intercombination lines (y, x: $1s^2\ ^1S_0$–$1s2p\ ^3P_{1,2}$, 568.6 eV): and the resonance line (w: $1s^2\ ^1S_0$–$1s2p\ ^1P_1$, 574.0 eV). The product of the transition cross-section and branching ratio at a velocity of 400 kms^{-1} are 34 $\times\ 10^{-16} cm^2$, 10 $\times\ 10^{-16}\ cm^2$, and 11 $\times\ 10^{-16} cm^2$, for the forbidden, intercombination,

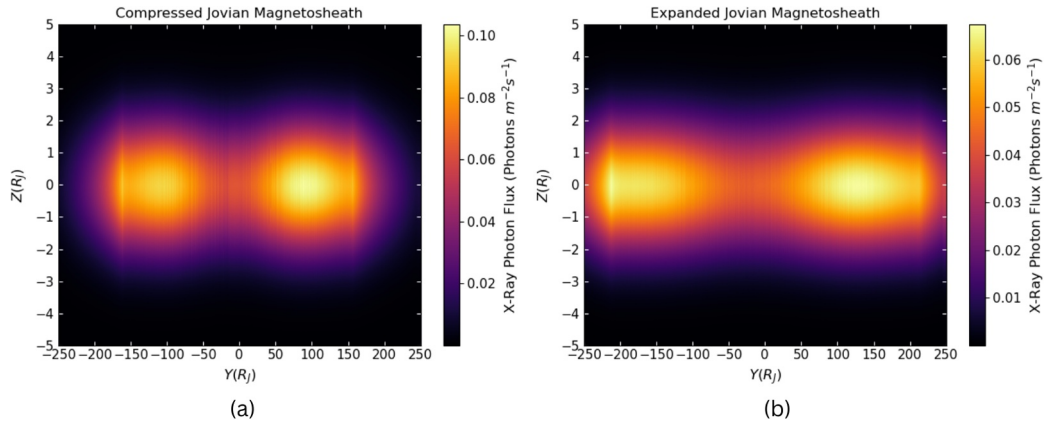

Figure 3. The top figures show the volume emission rates throughout the magnetosheath in the equatorial plane for a compressed (a) and expanded (b) 2D magnetosheath. The bottom figures show the photon flux leaving a plane normal to the nose of the bow shock in the equatorial plane for a compressed (c) and expanded (d) scenario. The emissions have an imposed $z = \pm 1$ to show structure.

and resonance lines respectively (Bodewits, D. et al., 2007). The OVII triplet involves a charge exchange between solar wind O^{7+} and H from within the Jovian system, leading to resultant species of H^{+} and O^{6+}.

3. Application of the Model to a SMILE SXI-Like Orbiting Instrument

The model was computed under two dynamic pressure scenarios applying the 10th and 90th percentiles from Ulysses solar wind data at 5.2 AU (Ebert et al., 2014). The 10th percentile has a value of 0.021 nPa and the 90th percentile is 0.167 nPa. The same value of dynamic pressure is imposed on the bow shock and magnetopause for each calculation. Density values are then computed for the 3D and 2D models and subsequently, volumetric emission rates (P_{sqj} in Equation 1). The volumetric emission rates in the equatorial plane are shown in Figures 3c and 3d. The emissions are then integrated along the JSM x-axis to produce a flux out of the bow shock surface. These flux estimations are shown in Figures 3a and 3b for the 2D model (with an imposed thickness of ±1z to show structure, and Figures 4a and 4b for 3D model. To interpret the results, we must define an observation point. For this, we assume that the SMILE soft x-ray imager (SXI) detector will observe the Jovian magnetosheath from the minimum distance to capture the emission region within its largest field of view (FOV) angle, as per its specifications from Soman et al. (2018). The maximum size of the emission region occurs during the low-pressure scenario and has a width of approximately 350 R_J assuming an FOV angle of 26.5°,the minimum distance is set as 744 R_J. Another option would be to position the spacecraft at Jupiter's Lagrange point 1 as this would provide a semi-stable observation position, this can be estimated using the radius of the Hill sphere

$$r \approx R \sqrt[3]{\frac{M_2}{3M_1}} \tag{5}$$

where R is the average Solar-Jupiter distance, M_1 is the mass of Jupiter, M_2 is the mass of the sun and r is the Hill sphere radius. The L1 distance from Equation 5 is 1,625 R_J or 0.76 AU which is 2.2 times larger than our minimum distance, although expected observation times would remain relatively consistent, the pixel scale in the resultant image would increase, reducing the ability to distinguish smaller scale features within the magnetosheath.

Integration times are calculated based on the assumption that one incident photon per pixel in the SXI is the minimum intensity required to produce an image. Therefore, the distance scaled flux is summed in the 2D model, after imposing a thickness of 1 R_J in the $\pm z$ direction, to provide the total flux which is then used to calculate integration times. For an expanded magnetosheath, integration times are calculated to be 2.4×10^8 seconds (6,700 Jovian rotations) and for a compressed magnetosheath 9.7×10^7 seconds (2,700 Jovian rotations). These calculated exposure times in the 2D model are much larger than the rotational period of Jupiter, and significantly longer than the timescale of other processes that occur in the magnetosheath.

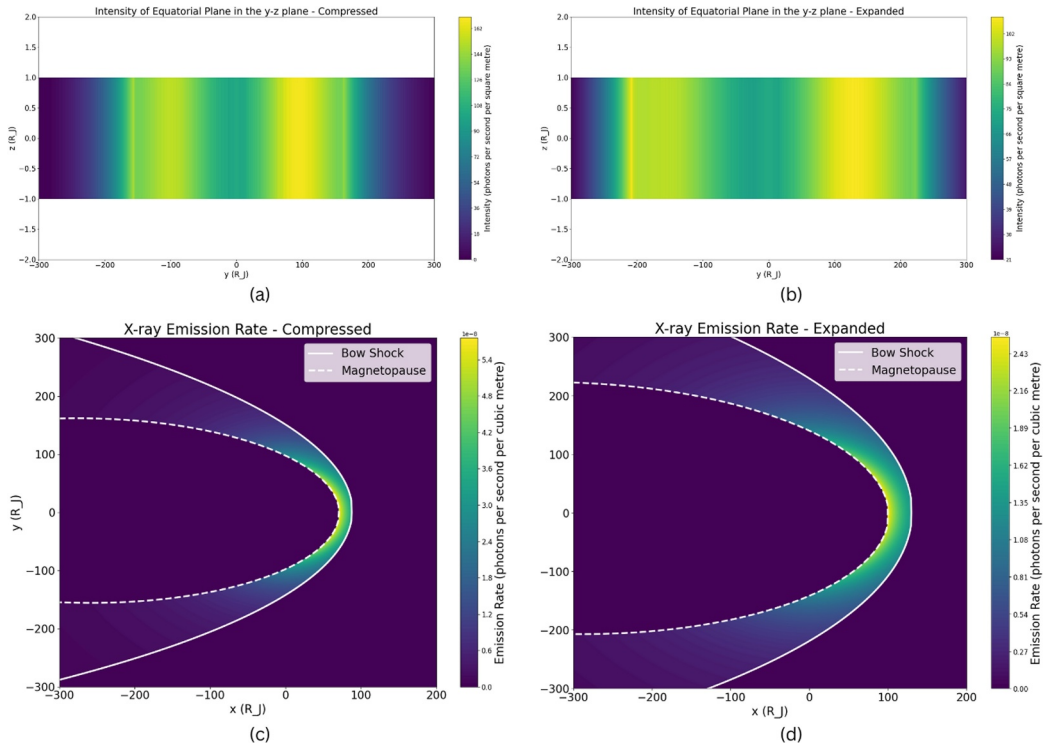

Figure 4. X-ray photon flux (photons $m^{-2}s^{-1}$) through a plane normal to the bow shock nose in the Jovian equatorial region (± 4 R_J) due to Solar Wind Charge eXchange between O VII and H in the magnetosheath calculated by the 3D model for a compressed (a) and expanded (b) scenario.

For the 3D model, an imaging model is developed to allow an observation from an arbitrary point, defined in spherical coordinates centered at Jupiter. The intensity from each point is projected to a plane on the edge of a simulation box, perpendicular to the observation point line of sight. The largest distance from the bow shock to the plane only results in a 5.2% decrease in flux, however, as the intensities are weakest in these regions the loss due to this assumption is negligible. As the 3D model is formed using a grid with finite resolution, we assume that each point on the 2D flux plane represents a tile with a uniform emission rate to form a complete surface. The FOV of the SMILE SXI (Sembay et al., 2024) is mapped onto the plane and the flux is summed and scaled with distance to calculate a whole detector count rate. We perform our tests with the following observation point in spherical coordinates: $\theta = 90°$, $\phi = 0°$. This approximates a position typical to the planned SMILE trajectory, as it is beneficial to observe the magnetosheath nose region from a high altitude to reduce noise from planetary sources, along with reducing the requirement for a large vertical FOV and increasing the count rate compared to a front on observation as seen in Figures 3 and 4. The area captured by SXI's FOV is shown in Figure 5a. This is then repeated for the Einstein Probe WXT (Yuan et al., 2022), BepiColombo MIXS-C (Fraser et al., 2010) and three theoretical imagers, the results are shown in Figure 5b and details of the FOV and effective area of each imager in Table 1. We selected these spacecraft as representative examples of existing X-ray detectors. In our count-rate calculations, we adopt a simple scaling with effective area; while incorporating each detector's detailed spectral response would introduce minor adjustments, it would not alter our overall conclusions. Likewise, although the instruments differ substantially in design and intended use, differences we have not modeled here, the primary goal of this study is merely to assess the viability of such observations. Full technical specifications for each instrument may be found in Sembay et al. (2024); Yuan et al. (2022); Fraser et al. (2010), and references therein. The imaging model is verified by applying it to an Earth magnetosheath model and comparing to simulated data for the SMILE SXI instrument, by which we estimate that all counts per minute calculations have an error of approximately an order of magnitude. All calculations are computed for a compressed scenario, as this provides a higher photon flux and allows a spacecraft to be positioned closer to the magnetosheath.

Estimated peak whole detector counts per minute are on the order of $10^{-5\pm1}$ for MIXS-C, $10^{-4\pm1}$ for SXI, and $10^{-3\pm1}$ for WXT, as can be seen in Figure 5b. Using two measurements of the diffuse soft x-ray background for

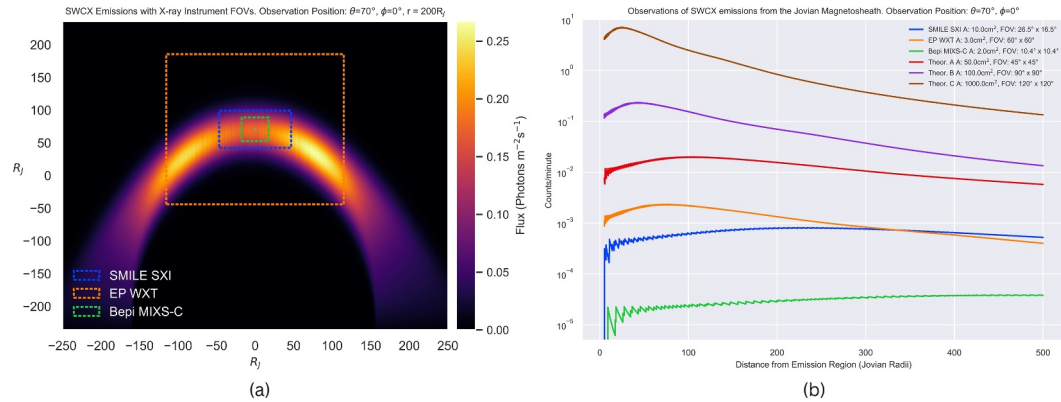

Figure 5. (a) Shows the FOVs of SMILE soft x-ray imager (SXI) (blue), Einstein Probe WXT (orange) and Bepi MIXS-C (green) projected onto a compressed magnetosheath emissions map from an observation point of $\theta = 70°$, $\phi = 0°$ and $r = 200R_J$. (b) Shows how the whole detector counts per minute vary with distance for SXI, WXT, MIXS-C and three theoretical detectors when viewed from a polar angle of 70° in a compressed magnetosheath scenario.

OVII, 2 photons s^{-1} cm^{-2} sr^{-1} (Yoshino et al., 2009) and 4.8 photons s^{-1} cm^{-2} sr^{-1} (McCammon et al., 2002), we calculate that the emissions from the Jovian magnetosheath is outshined by the diffuse background by 10^4-4 × 10^5 × for each detector, real and theoretical.

4. Discussion

Several assumptions made within this study mean that the calculated emissions are likely to represent a lower bound to emissions from the physical system itself. First, only the OVII triplet emission is considered. Several other emission lines would be present such as nitrogen and carbon lines, other oxygen lines like the OVIII 2p-1s 653.2 eV emission and possibly cascading emissions (e.g., OVIII to OVI). By constructing a more comprehensive model that incorporates the full chemistry of the solar wind and magnetospheric neutrals these emission lines could be included. However, as the OVII triplet is typically the brightest line, we estimate that the inclusion of a full spectrum would not result in an increase of more than a factor of approximately 12 in SWCX emissions. Consequently, it would not produce the more than 4+ orders of magnitude change needed to make a magnetosheath brighter than the diffuse soft x-ray background, let alone detectable within suitable timescales.

Second, magnetosheath flow velocities and temperature is assumed to be constant in the 3D model. In reality there is a positive velocity gradient from the magnetopause to the bow shock, and one would expect flow to be stagnated at the nose of the bow shock before accelerating back to typical solar wind velocities as plasma travels down toward the magnetotail. This would likely change the shape of the emission regions but its effect on the overall x-ray photon flux would be negligible. There is a possibility that the Jovian magnetosheath could be a source of O^{7+}. Our current understanding of Jupiter's polar x-ray aurora is that they are generated by the charge exchange mechanism, but we do not know how the O^{7+} ions become so highly charged. They could be produced in the atmosphere during precipitation or in the magnetosphere (Houston et al., 2018). If the latter, then they must be very close to the magnetopause in order to precipitate into the polar cap region. If this is the case, there could be a significantly higher population of high charge state heavy ions near the magnetopause which could significantly alter our estimates. This presents an interesting avenue for further research.

Despite these assumptions and simplifications we still conclude that the Jovian magnetosheath should not be the target of an x-ray study. Emission rates are 10^4-4 × 10^5 times lower than the diffuse soft x-ray background when observed from a local orbiting instrument, and thus are unobservable and would contribute a negligible addition to the background noise when observing other x-ray sources in the Jovian system which have significantly

Table 1
The Effective Area at 1 keV and Field of View (FOV) for the Three Real (SXI, MIXS-C, and WXT) and Three Theoretical (A, B, and C) Spacecraft Used for Calculating Whole Detector Counts per Minute From the Jovian Magnetosheath, as Seen in Figure 5b

Spacecraft	Effective area (cm^2)	FOV
SMILE SXI	10.0	26.5° × 16.5°
Einstein Probe WXT	3.0	60.0° × 60.0°
BepiColumbo MIXS-C	2.0	10.4° × 10.4°
Theoretical A	50.0	45.0° × 45.0°
Theoretical B	100.0	90.0° × 90.0°
Theoretical C	1,000.0	120.0° × 120.0°

higher emission rates. Some examples include: bremsstrahlung and CX emissions from the Io plamsa torus, reflected solar x-rays from the Jovian disk, polar auroral x-ray emissions, and x-ray fluorescence from the Jovian moons. Therefore, despite the magnetosheath not being a viable target, Jupiter still has many bright x-ray sources that should be the focus of future x-ray missions.

A better possible candidate for magnetosheath SWCX observations would be Saturn. It too has internal neutral sources from cryovolcanoes on Enceladus. Additionally, its lower gravity results in a more extended exosphere than Jupiter, meaning it has a neutral dominated system. These two factors in combination with its significantly more compact magnetosphere would likely result in a higher magnetosheath SWCX emission rates but this would require further study to confirm.

5. Conclusion

This study set out to determine the viability of imaging the Jovian magnetosheath with a soft x-ray instrument. This was achieved by producing a model of the Jovian magnetosheath using polynomial boundary equations derived by Joy et al. (2002) and defining neutral and charged particle populations from numerical models and Juno in situ measurements. It was found that the peak O VII triplet emissions are on the order of 10^{-1} photons m^{-2} s^{-1} in a compressed magnetosheath and 6×10^{-2} photons m^{-2} s^{-1} in an expanded magnetosheath. Assuming a spacecraft identical to the SMILE mission, located at the minimum distance to capture the entire emission region ($744\,R_J$), integration times range from 2,700 to 6,700 Jovian rotations in the 2D model. The 3D model estimates that the whole detector counts per minute are on the order of $10^{-5\pm1}$ for MIXS-C, $10^{-4\pm1}$ for SXI, and $10^{-3\pm1}$ for WXT. When comparing to the diffuse soft x-ray background of 2–4.8 photons s^{-1} cm^{-2} sr^{-1}, magnetosheath emissions are 10^4-4×10^5 times weaker, based on these estimations we state that the Jovian magnetosheath is not feasibly observable. Our estimated intensities are likely to be an underestimate, however applying a more detailed description of the system would lead to variations up to about one order of magnitude, and not the needed 4+ orders of magnitude x-ray flux enhancement needed to increase the signal to noise ratio to be greater than one. Therefore, magnetosheath emissions, while likely to exist, would provide only a negligible addition to the diffuse soft x-ray background and still provide a low noise floor in the x-ray band when locally observing the numerous x-ray bright sources in the Jovian system.

Data Availability Statement

The software used to produce Figures 2–5 can be found at Leppard and Patrick (2025). No data sets were used in this study.

Acknowledgments
LR acknowledges STFC grant to Lancaster University (ST/Y002148/1). WD acknowledges the STFC Ernest Rutherford Fellowship (ST/W003449/1). ZY acknowledges the General Program of the National Natural Science Foundation of China (Grant 42374212), the Research Grants Council (RGC) General Research Fund (Grant 17309124) and Project (JLFS/P-702/24) of Hong Kong RGC Co-funding Mechanism on Joint Laboratories with the Chinese Academy of Science.

References

Bagenal, F., & Delamere, P. A. (2011). Flow of mass and energy in the magnetospheres of jupiter and saturn. *Journal of Geophysical Research*, *116*(A5), A05209. https://doi.org/10.1029/2010ja016294

Barbosa, D. (1990). Bremsstrahlung x rays from jovian auroral electrons. *Journal of Geophysical Research*, *95*(A9), 14969–14976. https://doi.org/10.1029/ja095ia09p14969

Bhardwaj, A., Branduardi-Raymont, G., Elsner, R. F., Gladstone, G. R., Ramsay, G., Rodriguez, P., et al. (2005). Solar control on jupiter's equatorial x-ray emissions: 26–29 november 2003 xmm-Newton observation. *Geophysical Research Letters*, *32*(3), L03S08. https://doi.org/10.1029/2004gl021497

Bhardwaj, A., Elsner, R. F., Gladstone, G. R., Cravens, T. E., Lisse, C. M., Dennerl, K., et al. (2007). X-rays from solar system objects. *Planetary and Space Science*, *55*(9), 1135–1189. https://doi.org/10.1016/j.pss.2006.11.009

Bhardwaj, A., & Gladstone, G. R. (2000). Auroral emissions of the giant planets. *Reviews of Geophysics*, *38*(3), 295–353. https://doi.org/10.1029/1998rg000046

Bochsler, P. (2007). Minor ions in the solar wind. *Astronomy and Astrophysics Review*, *14*, 1–40. https://doi.org/10.1007/s00159-006-0002-x

Bodewits, D., Christian, D. J., Torney, M., Dryer, M., Lisse, C. M., Dennerl, K., et al. (2007). Spectral analysis of the chandra comet survey. *A&A*, *469*(3), 1183–1195. https://doi.org/10.1051/0004-6361:20077410

Branduardi-Raymont, G., Bhardwaj, A., Elsner, R., Gladstone, G., Ramsay, G., Rodriguez, P., et al. (2007a). Latest results on jovian disk x-rays from xmm-Newton. *Planetary and Space Science*, *55*(9), 1126–1134. https://doi.org/10.1016/j.pss.2006.11.017

Branduardi-Raymont, G., Bhardwaj, A., Elsner, R., Gladstone, G., Ramsay, G., Rodriguez, P., et al. (2007b). A study of jupiter's aurorae with xmm-Newton. *Astronomy and Astrophysics*, *463*(2), 761–774. https://doi.org/10.1051/0004-6361:20066406

Branduardi-Raymont, G., Bhardwaj, A., Elsner, R., & Rodriguez, P. (2010). X-Rays from saturn: A study with xmm-Newton and chandra over the years 2002–05. *Astronomy and Astrophysics*, *510*, A73. https://doi.org/10.1051/0004-6361/200913110

Branduardi-Raymont, G., Elsner, R., Gladstone, G., Ramsay, G., Rodriguez, P., Soria, R., & Waite, J. (2004). First observation of jupiter by xmm-Newton. *Astronomy and Astrophysics*, *424*(1), 331–337. https://doi.org/10.1051/0004-6361:20041149

Branduardi-Raymont, G., Elsner, R. F., Galand, M., Grodent, D., Cravens, T., Ford, P., et al. (2008). Spectral morphology of the x-ray emission from jupiter's aurorae. *Journal of Geophysical Research*, *113*(A2), A02202. https://doi.org/10.1029/2007ja012600

Branduardi-Raymont, G., Wang, C., Escoubet, C., Adamovic, M., Agnolon, D., Berthomier, M., et al. (2018). Smile definition study report.
Brown, G., Beiersdorfer, P., Chen, H., Clementson, J., Frankel, M., Gu, M., et al. (2009). Studies of x-ray production following charge exchange recombination between highly charged ions and neutral atoms and molecules. *Journal of Physics: Conference Series*, *163*, 012–052. https://doi.org/10.1088/1742-6596/163/1/012052
Carter, J., & Sembay, S. (2008). Identifying xmm-Newton observations affected by solar wind charge exchange. part i. *Astronomy and Astrophysics*, *489*(2), 837–848. https://doi.org/10.1051/0004-6361:200809997
Carter, J., Sembay, S., & Read, A. (2011). Identifying xmm-Newton observations affected by solar wind charge exchange–part ii. *Astronomy and Astrophysics*, *527*, A115. https://doi.org/10.1051/0004-6361/201015817
Cowley, S., Badman, S., Imber, S., & Milan, S. (2008). Comment on "jupiter: A fundamentally different magnetospheric interaction with the solar wind" by dj mccomas and f. bagenal. *Geophysical Research Letters*, *35*(10), L10101. https://doi.org/10.1029/2007gl032645
Cravens, T. (1997). Comet hyakutake x-ray source: Charge transfer of solar wind heavy ions. *Geophysical Research Letters*, *24*(1), 105–108. https://doi.org/10.1029/96gl03780
Cravens, T., Robertson, I., & Snowden, S. (2001). Temporal variations of geocoronal and heliospheric x-ray emission associated with the solar wind interaction with neutrals. *Journal of Geophysical Research*, *106*(A11), 24883–24892. https://doi.org/10.1029/2000ja000461
Delamere, P., & Bagenal, F. (2010). Solar wind interaction with jupiter's magnetosphere. *Journal of Geophysical Research*, *115*(A10), A10201.
Dennerl, K. (2002). Discovery of x–rays from mars with chandra. *Astronomy and Astrophysics*, *394*(3), 1119–1128. https://doi.org/10.1051/0004-6361:20021116
Dennerl, K., Burwitz, V., Englhauser, J., Lisse, C., & Wolk, S. (2002). Discovery of x–rays from venus with chandra. *Astronomy and Astrophysics*, *386*(1), 319–330. https://doi.org/10.1051/0004-6361:20020097
Desroche, M., Bagenal, F., Delamere, P., & Erkaev, N. (2012). Conditions at the expanded jovian magnetopause and implications for the solar wind interaction. *Journal of Geophysical Research*, *117*(A7), A07202. https://doi.org/10.1029/2012ja017621
Dunn, W. R. (2022). X-ray emissions from the jovian system. *arXiv preprint arXiv:2208.13455*, 1–56. https://doi.org/10.1007/978-981-16-4544-0_73-1
Dunn, W. R., Branduardi-Raymont, G., Carter-Cortez, V., Campbell, A., Elsner, R., Ness, J.-U., et al. (2020). Jupiter's x-ray emission during the 2007 solar minimum. *Journal of Geophysical Research: Space Physics*, *125*(6), e2019JA027219. https://doi.org/10.1029/2019ja027219
Dunn, W. R., Branduardi-Raymont, G., Elsner, R. F., Vogt, M. F., Lamy, L., Ford, P. G., et al. (2016). The impact of an icme on the jovian x-ray aurora. *Journal of Geophysical Research: Space Physics*, *121*(3), 2274–2307. https://doi.org/10.1002/2015ja021888
Dunn, W. R., Branduardi-Raymont, G., Ray, L., Jackman, C., Kraft, R., Elsner, R., et al. (2017). The independent pulsations of jupiter's northern and southern x-ray auroras. *Nature Astronomy*, *1*(11), 758–764. https://doi.org/10.1038/s41550-017-0262-6
Dunn, W. R., Gray, R., Wibisono, A., Lamy, L., Louis, C., Badman, S., et al. (2020). Comparisons between jupiter's x-ray, uv and radio emissions and in-situ solar wind measurements during 2007. *Journal of Geophysical Research: Space Physics*, *125*(6), e2019JA027222. https://doi.org/10.1029/2019ja027222
Ebert, R. W., Bagenal, F., McComas, D. J., & Fowler, C. M. (2014). A survey of solar wind conditions at 5 au: A tool for interpreting solar wind-magnetosphere interactions at jupiter. *Frontiers in Astronomy and Space Sciences*, *1*. https://doi.org/10.3389/fspas.2014.00004
Elsner, R. F., Gladstone, G. R., Waite, J. H., Crary, F. J., Howell, R. R., Johnson, R. E., et al. (2002). Discovery of soft x-ray emission from io, europa, and the io plasma torus. *The Astrophysical Journal*, *572*(2), 1077–1082. https://doi.org/10.1086/340434
Elsner, R. F., Lugaz, N., Waite Jr, J., Cravens, T., Gladstone, G., Ford, P., et al. (2005). Simultaneous chandra x ray, hubble space telescope ultraviolet, and ulysses radio observations of jupiter's aurora. *Journal of Geophysical Research*, *110*(A1), A01207. https://doi.org/10.1029/2004ja010717
Ezoe, Y., Ishikawa, K., Ohashi, T., Miyoshi, Y., Terada, N., Uchiyama, Y., & Negoro, H. (2010). Discovery of diffuse hard x-ray emission around jupiter with suzaku. *The Astrophysical Journal Letters*, *709*(2), L178–L182. https://doi.org/10.1088/2041-8205/709/2/l178
Feng, E., Zhang, B., Yao, Z., Delamere, P. A., Zheng, Z., Dunn, W. R., & Ye, S.-Y. (2023). Variation of the jovian magnetopause under constant solar wind conditions: Significance of magnetodisc dynamics. *Geophysical Research Letters*, *50*(12), e2023GL104046. https://doi.org/10.1029/2023gl104046
Fraser, G., Carpenter, J., Rothery, D., Pearson, J., Martindale, A., Huovelin, J., et al. (2010). The mercury imaging x-ray spectrometer (mixs) on bepicolombo. *Planetary and Space Science*, *58*(1–2), 79–95. https://doi.org/10.1016/j.pss.2009.05.004
Gladstone, G., Waite Jr, J., Grodent, D., Lewis, W., Crary, F., Elsner, R. F., et al. (2002). A pulsating auroral x-ray hot spot on jupiter. *Nature*, *415*(6875), 1000–1003. https://doi.org/10.1038/4151000a
Guo, J., Sun, T., Lu, S., Lu, Q., Lin, Y., Wang, X., et al. (2024). Global hybrid simulations of soft x-ray emissions in the earth's magnetosheath. *Earth and Planetary Physics*, *8*(1), 47–58. https://doi.org/10.26464/epp2023053
Gurnett, D. A., Kurth, W. S., Hospodarsky, G. B., Persoon, A., Zarka, P., Lecacheux, A., et al. (2002). Control of jupiter's radio emission and aurorae by the solar wind. *Nature*, *415*(6875), 985–987. https://doi.org/10.1038/415985a
Hess, S., Echer, E., & Zarka, P. (2012). Solar wind pressure effects on jupiter decametric radio emissions independent of io. *Planetary and Space Science*, *70*(1), 114–125. https://doi.org/10.1016/j.pss.2012.05.011
Hess, S. L., Echer, E., Zarka, P., Lamy, L., & Delamere, P. (2014). Multi-instrument study of the jovian radio emissions triggered by solar wind shocks and inferred magnetospheric subcorotation rates. *Planetary and Space Science*, *99*, 136–148. https://doi.org/10.1016/j.pss.2014.05.015
Houston, S., Ozak, N., Young, J., Cravens, T., & Schultz, D. (2018). Jovian auroral ion precipitation: Field-aligned currents and ultraviolet emissions. *Journal of Geophysical Research: Space Physics*, *123*(3), 2257–2273. https://doi.org/10.1002/2017ja024872
Joy, S., Kivelson, M., Walker, R., Khurana, K., Russell, C., & Ogino, T. (2002). Probabilistic models of the jovian magnetopause and bow shock locations. *Journal of Geophysical Research*, *107*(A10), SMP–17. https://doi.org/10.1029/2001ja009146
Küntz, K., Koutroumpa, D., R Dunn, W., Foster, A., S Porter, F., G Sibeck, D., & Walsh, B. (2024). The magnetosheath at high spectral resolution. *Earth and Planetary Physics*, 234–246.
Leppard, F., & Patrick, A. (2025). Data files/software: Estimating solar wind charge exchange generated soft x-rays in the jovian magnetosheath. *Zenodo*. https://doi.org/10.5281/zenodo.13939387
Lisse, C., Christian, D., Wolk, S., Günther, H., Chen, C., & Grady, C. (2017). Chandra characterization of x-ray emission in the young f-star binary system hd 113766. *The Astronomical Journal*, *153*(2), 62. https://doi.org/10.3847/1538-3881/153/2/62
Lisse, C., Dennerl, K., Englhauser, J., Harden, M., Marshall, F., Mumma, M., et al. (1996). Discovery of x-ray and extreme ultraviolet emission from comet c/hyakutake 1996 b2. *Science*, *274*(5285), 205–209. https://doi.org/10.1126/science.274.5285.205
Lodders, K. (2019). Solar elemental abundances. *arXiv preprint arXiv:1912.00844*.
McCammon, D., Almy, R., Apodaca, E., Bergmann Tiest, W., Cui, W., Deiker, S., et al. (2002). A high spectral resolution observation of the soft x-ray diffuse background with thermal detectors. *The Astrophysical Journal*, *576*(1), 188–203. https://doi.org/10.1086/341727

McComas, D., & Bagenal, F. (2007). Jupiter: A fundamentally different magnetospheric interaction with the solar wind. *Geophysical Research Letters*, *34*(20), L20106. https://doi.org/10.1029/2007gl031078

Metzger, A. E., Gilman, D. A., Luthey, J. L., Hurley, K. C., Schnopper, H. W., Seward, F. D., & Sullivan, J. D. (1983). The detection of x rays from jupiter. *Journal of Geophysical Research*, *88*(A10), 7731–7741. https://doi.org/10.1029/ja088ia10p07731

Mori, K., Hailey, C., Bridges, G., Mandel, S., Garvin, A., Grefenstette, B., et al. (2022). Observation and origin of non-thermal hard x-rays from jupiter. *Nature Astronomy*, *6*(4), 442–448. https://doi.org/10.1038/s41550-021-01594-8

Ness, J.-U., Mewe, R., Schmitt, J., Raassen, A., Porquet, D., Kaastra, J., et al. (2001). Helium-like triplet density diagnostics-applications to chandra-letgs x-ray observations of capella and procyon. *Astronomy and Astrophysics*, *367*(1), 282–296. https://doi.org/10.1051/0004-6361:20000419

Nichols, J., Badman, S. V., Bagenal, F., Bolton, S., Bonfond, B., Bunce, E., et al. (2017). Response of jupiter's auroras to conditions in the interplanetary medium as measured by the hubble space telescope and juno. *Geophysical Research Letters*, *44*(15), 7643–7652. https://doi.org/10.1002/2017gl073029

Nichols, J., Clarke, J., Gérard, J.-C., Grodent, D., & Hansen, K. (2009). Variation of different components of jupiter's auroral emission. *Journal of Geophysical Research*, *114*(A6), A06210. https://doi.org/10.1029/2009ja014051

Nulsen, S., Kraft, R., Germain, G., Dunn, W., Tremblay, G., Beegle, L., et al. (2020). X-Ray emission from jupiter's galilean moons: A tool for determining their surface composition and particle environment. *The Astrophysical Journal*, *895*(2), 79. https://doi.org/10.3847/1538-4357/ab8cbc

Ogino, T., Walker, R. J., & Kivelson, M. G. (1998). A global magnetohydrodynamic simulation of the jovian magnetosphere. *Journal of Geophysical Research*, *103*(A1), 225–235. https://doi.org/10.1029/97ja02247

Porquet, D., Dubau, J., & Grosso, N. (2010). He-like ions as practical astrophysical plasma diagnostics: From stellar coronae to active galactic nuclei. *Space Science Reviews*, *157*(1–4), 103–134. https://doi.org/10.1007/s11214-010-9731-2

Raab, W., Branduardi-Raymont, G., Wang, C., Dai, L., Donovan, E., Enno, G., et al. (2016). Smile: A joint esa/cas mission to investigate the interaction between the solar wind and earth's magnetosphere. In *Space telescopes and instrumentation 2016: Ultraviolet to gamma ray* (Vol. 9905). https://doi.org/10.1117/12.2231984

Ranquist, D., Bagenal, F., Wilson, R., Hospodarsky, G., Ebert, R., Allegrini, F., et al. (2019). Survey of jupiter's dawn magnetosheath using juno. *Journal of Geophysical Research: Space Physics*, *124*(11), 9106–9123. https://doi.org/10.1029/2019ja027382

Robertson, I., Collier, M., Cravens, T., & Fok, M.-C. (2006). X-ray emission from the terrestrial magnetosheath including the cusps. *Journal of Geophysical Research*, *111*(A12), A12105. https://doi.org/10.1029/2006ja011672

Samsonov, A., Branduardi-Raymont, G., Sembay, S., Read, A., Sibeck, D., & Rastaetter, L. (2023). Simulation of the smile soft x-ray imager response to a southward interplanetary magnetic field turning. *Earth and Planetary Physics*, *8*(1), 39–46. https://doi.org/10.26464/epp2023058

Sembay, S., Alme, A. L., Agnolon, D., Arnold, T., Beardmore, A., Margeli, A. B. B., et al. (2024). The soft x-ray imager (sxi) on the smile mission. *Earth and Planetary Physics*, *8*(1), 5–14. https://doi.org/10.26464/epp2023067

Sibeck, D. G., Allen, R., Aryan, H., Bodewits, D., Brandt, P., Branduardi-Raymont, G., et al. (2018). Imaging plasma density structures in the soft x-rays generated by solar wind charge exchange with neutrals. *Space Science Reviews*, *214*(4), 1–124. https://doi.org/10.1007/s11214-018-0504-7

Siscoe, G. L., & Summers, D. (1981). Centrifugally driven diffusion of iogenic plasma. *Journal of Geophysical Research*, *86*(A10), 8471–8479. https://doi.org/10.1029/ja086ia10p08471

Smith, H., Crary, F. J., Dougherty, M. K., Perry, M. E., Roussos, E., Simon, S., & Tokar, R. L. (2018). Enceladus and its influence on Saturn's magnetosphere. In P. M. Schenk, R. N. Clark, C. J. A. Howett, A. J. Verbiscer, & J. H. Waite (Eds.), *Enceladus and the icy moons of saturn* (p. 211). https://doi.org/10.2458/azu_uapress_9780816537075-ch011

Smith, H., Johnson, R., Perry, M., Mitchell, D., McNutt, R., & Young, D. (2010). Enceladus plume variability and the neutral gas densities in saturn's magnetosphere. *Journal of Geophysical Research*, *115*(A10), A10252. https://doi.org/10.1029/2009ja015184

Smith, H., Johnson, R., & Shematovich, V. (2004). Titan's atomic and molecular nitrogen tori. *Geophysical Research Letters*, *31*(16), L16804. https://doi.org/10.1029/2004gl020580

Smith, H., Johnson, R., Sittler, E., Shappirio, M., Reisenfeld, D., Tucker, O., et al. (2007). Enceladus: The likely dominant nitrogen source in saturn's magnetosphere. *Icarus*, *188*(2), 356–366. https://doi.org/10.1016/j.icarus.2006.12.007

Smith, H., Koga, R., Tsuchiya, F., & Dols, V. J. (2022). Insight into io enabled by characterization of its neutral oxygen torus. *Journal of Geophysical Research: Space Physics*, *127*(8), e2022JA030581. https://doi.org/10.1029/2022JA030581

Smith, H., Mitchell, D., Johnson, R., Mauk, B., & Smith, J. (2019). Europa neutral torus confirmation and characterization based on observations and modeling. *The Astrophysical Journal*, *871*(1), 69. https://doi.org/10.3847/1538-4357/aaed38

Smith, H., & Richardson, J. (2021). The 3d structure of saturn magnetospheric neutral tori produced by the enceladus plumes. *Journal of Geophysical Research: Space Physics*, *126*(3), e2020JA028775. https://doi.org/10.1029/2020ja028775

Soman, M., Hall, D., Holland, A., Burgon, R., Buggey, T., Skottfelt, J., et al. (2018). The smile soft x-ray imager (sxi) ccd design and development. *Journal of Instrumentation*, *13*(1), C01022. https://doi.org/10.1088/1748-0221/13/01/c01022

Stahara, S., Rachiele, R., Spreiter, J., & Slavin, J. (1989). A three dimensional gasdynamic model for solar wind flow past nonaxisymmetric magnetospheres: Application to jupiter and saturn. *Journal of Geophysical Research*, *94*(A10), 13353–13365.

Stone, E. C., Frandsen, A., Mewaldt, R., Christian, E., Margolies, D., Ormes, J., & Snow, F. (1998). The advanced composition explorer. *Space Science Reviews*, *86*, 1–22. https://doi.org/10.1007/978-94-011-4762-0_1

Sun, T., Wang, C., Connor, H. K., Jorgensen, A. M., & Sembay, S. (2020). Deriving the magnetopause position from the soft x-ray image by using the tangent fitting approach. *Journal of Geophysical Research: Space Physics*, *125*(9), e2020JA028169. https://doi.org/10.1029/2020ja028169

Sun, T., Wang, C., Sembay, S., Lopez, R., Escoubet, C., Branduardi-Raymont, G., et al. (2019). Soft x-ray imaging of the magnetosheath and cusps under different solar wind conditions: Mhd simulations. *Journal of Geophysical Research: Space Physics*, *124*(4), 2435–2450. https://doi.org/10.1029/2018ja026093

Waite, J., Jr., Bagenal, F., Seward, F., Na, C., Gladstone, G., Cravens, T., et al. (1994). Rosat observations of the jupiter aurora. *Journal of Geophysical Research*, *99*(A8), 14799–14809. https://doi.org/10.1029/94ja01005

Wang, C., & Branduardi-Raymond, G. (2018). Progress of solar wind magnetosphere ionosphere link explorer (smile) mission. *Chinese Journal of Space Science*, *38*(5), 657–661. https://doi.org/10.11728/cjss2018.05.657

Wang, C., & Sun, T. (2022). Methods to derive the magnetopause from soft x-ray images by the smile mission. *Geoscience Letters*, *9*(1), 30. https://doi.org/10.1186/s40562-022-00240-z

Weigt, D., Jackman, C., Dunn, W., Gladstone, G., Vogt, M., Wibisono, A., et al. (2020). Chandra observations of jupiter's x-ray auroral emission during juno apojove 2017. *Journal of Geophysical Research: Planets*, *125*(4), e2019JE006262. https://doi.org/10.1029/2019je006262

Wibisono, A., Branduardi-Raymont, G., Coates, A., Dunn, W., & French, R. (2023). Jupiter's equatorial x-ray emissions over two solar cycles. *Monthly Notices of the Royal Astronomical Society*, *521*(4), 5596–5603. https://doi.org/10.1093/mnras/stad905

Wibisono, A., Branduardi-Raymont, G., Coates, A., Dunn, W. R., Haythornthwaite, R., Kimura, T., et al. (2020). Searching for signatures of tail reconnection and plasma injection events in jupiter's x-ray aurora. *Tech. Rep. Copernicus Meetings*.

Wibisono, A., Branduardi-Raymont, G., Dunn, W., Kimura, T., Coates, A., Grodent, D., et al. (2021). Jupiter's x-ray aurora during uv dawn storms and injections as observed by xmm–Newton, hubble, and hisaki. *Monthly Notices of the Royal Astronomical Society*, *507*(1), 1216–1228. https://doi.org/10.1093/mnras/stab2218

Yao, Z., Bonfond, B., Grodent, D., Chané, E., Dunn, W., Kurth, W., et al. (2022). On the relation between auroral morphologies and compression conditions of jupiter's magnetopause: Observations from juno and the hubble space telescope. *Journal of Geophysical Research: Space Physics*, *127*(10), e2021JA029894. https://doi.org/10.1029/2021ja029894

Yao, Z., Dunn, W. R., Woodfield, E. E., Clark, G., Mauk, B. H., Ebert, R. W., et al. (2021). Revealing the source of jupiter's x-ray auroral flares. *Science Advances*, *7*(28), eabf0851. https://doi.org/10.1126/sciadv.abf0851

Yoshino, T., Mitsuda, K., Yamasaki, N. Y., Takei, Y., Hagihara, T., Masui, K., et al. (2009). Energy spectra of the soft x-ray diffuse emission in fourteen fields observed with suzaku. *Publications of the Astronomical Society of Japan*, *61*(4), 805–823. https://doi.org/10.1093/pasj/61.4.805

Yuan, W., Zhang, C., Chen, Y., & Ling, Z. (2022). The Einstein probe mission. In *Handbook of x-ray and gamma-ray astrophysics* (pp. 1–30). Springer.

Zhang, Y., Sun, T., Wang, C., Ji, L., Carter, J. A., Sembay, S., et al. (2022). Solar wind charge exchange soft x-ray emissions in the magnetosphere during an interplanetary coronal mass ejection compared to its driven sheath. *The Astrophysical Journal Letters*, *932*(1), L1. https://doi.org/10.3847/2041-8213/ac7521